

UDC 666.798:621.762.4

DOI: 10.15587/1729-4061.2021.245938

DETERMINING THE INFLUENCE OF ULTRA-DISPERSED ALUMINUM NITRIDE IMPURITIES ON THE STRUCTURE AND PHYSICAL-MECHANICAL PROPERTIES OF TOOL CERAMICS

Edwin Gevorkyan

Doctor of Technical Sciences, Professor*

Volodymyr Nerubatskyi

Corresponding author

PhD, Associate Professor

Department of Electrical Power Engineering, Electrical Engineering and Electromechanics**

E-mail: NVP9@i.ua

Volodymyr Chyshkala

PhD, Associate Professor

Department of Materials for Reactor Building and Physical Technologies

V. N. Karazin Kharkiv National University
Svobody sq., 4, Kharkiv, Ukraine, 61022

Yuriy Gutsalenko

Senior Researcher, Senior Lecturer

Department of Integrated Technologies of Mechanical Engineering named after M.F. Semko

National Technical University "Kharkiv Polytechnic Institute"
Kyrpychova str., 2, Kharkiv, Ukraine, 61002

Oksana Morozova

Postgraduate Student*

*Department of Wagon Engineering and Product Quality**

**Ukrainian State University of Railway Transport

Feierbakha sq., 7, Kharkiv, Ukraine, 61050

This paper considers features related to manufacturing the chromium oxide-based tool material. The process involved ultra-dispersed powders made of aluminum nitride. It has been established that the destruction of chromium oxide at high sintering temperatures is prevented through the reaction sintering of chromium oxide (Cr_2O_3) and aluminum nitride (AlN).

It was established that the structure of the composite depends both on the temperature and the duration of hot pressing. Thermodynamic calculations of the interaction between Cr_2O_3 and AlN showed that this interaction begins at a temperature of 1,300 °C. In contrast to hot pressing in the air, no CrN and Cr_2N compounds were formed in a vacuum. With increasing temperature, the content of Al_2O_3 in solid solution becomes maximum at a temperature of 1,700 °C in the case of hot pressing in the air while in vacuum the content of Al_2O_3 remains unchanged within the entire temperature range of 1,300–1,700 °C. When increasing the time of hot pressing to 30 minutes, the size of individual grains reaches 10 μm . It has been shown that in the sintering process involving Cr_2O_3 and AlN, the plasma-chemical synthesis produces the solid solution $(\text{Cr}, \text{Al})_2\text{O}_3$ at the interphase boundary, which improves the mechanical properties of the material.

The influence exerted on the quality of the machined surface of tempered hard steel when machining by the devised tool material based on chromium oxide with an optimal admixture of 15 wt % of ultra-dispersed aluminum nitride powder was investigated. It was determined that the quality of the machined hard steel surface improved compared to standard imported tool plates.

It was established that the resulting tool material, in addition to relatively high strength and crack resistance, also demonstrates high thermal conductivity, which favorably affects the quality of the machined steel surface, given that lubricants and coolants are not used during the cutting process

Keywords: hot pressing, tool material, aluminum nitride, chromium oxide, ultra-dispersed powder

Received date 04.10.2021

Accepted date 16.11.2021

Published date 22.12.2021

How to Cite: Gevorkyan, E., Nerubatskyi, V., Chyshkala, V., Gutsalenko, Y., Morozova, O. (2021). Determining the influence of ultra-dispersed aluminum nitride impurities on the structure and physical-mechanical properties of tool ceramics. Eastern-European Journal of Enterprise Technologies, 6 (12 (114)), 40–52. doi: <https://doi.org/10.15587/1729-4061.2021.245938>

1. Introduction

For machining, the quality of the cutting tool materials is one of the most important issues that need to be addressed. Increasing the productivity of the cutting tool can be achieved through the use of modern composite ceramic cutting materials [1]. These materials should demonstrate the following set of properties: high hardness, wear resistance, strength, impact viscosity, oxidation resistance [2, 3]. In addition, cutting tool materials must be able to withstand extreme cutting conditions

such as high temperature and friction between a workpiece and the cutting tool surface. This can be achieved through surface treatment, as well as by applying hot pressing and spark plasma sintering – two basic processes used to make such tools.

The availability of a variety of machined metals necessitates designing a wide range of cutting materials, each of which would have its specific application area [4, 5]. Potential fields of the practical application of various cutting materials depending on the cutting speed and feed rate are shown in Fig. 1 [6].

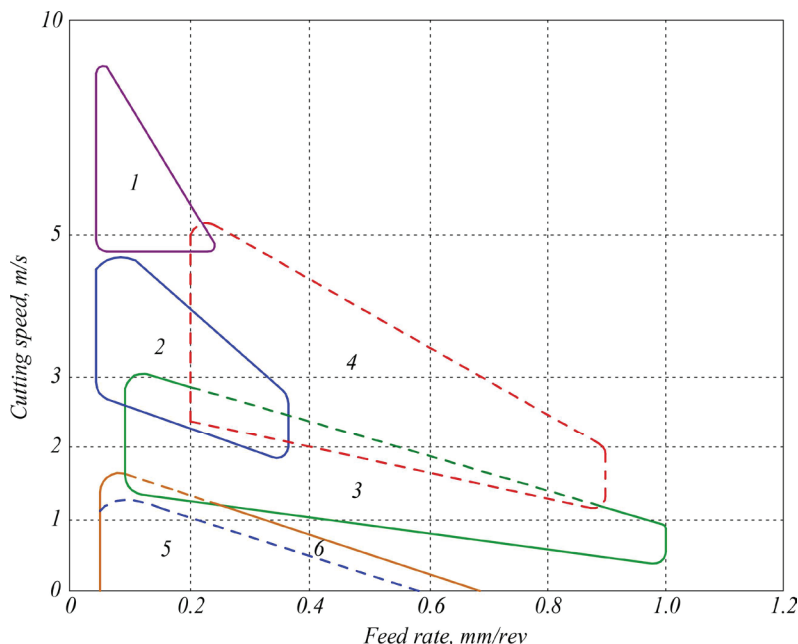


Fig. 1. Typical fields of the practical application of various cutting tools: 1 – ceramics; 2 – cermet; 3 – hard alloy; 4 – coated hard alloy; 5 – fast-cutting steel; 6 – fast-cutting coated steel

Fig. 1 shows that materials with higher high-temperature hardness can be used at high cutting speeds [7]; those with enhanced strength – at high feed rate values [8].

The wear resistance of the material is higher, the higher the hardness of the material [9, 10]. However, since different types of wear include the phenomena of diffusion, adhesion, electrochemical wear, depending on the material being machined and the conditions of machining, intense wear can be observed even in those materials that possess high hardness. In the modern process of metalworking, tools based on refractive compounds of four types are used: hard alloys, tungsten-free hard steels, carbide steels, and ceramics [11, 12].

Once we consider the dependence of the cutting speed on the mechanical characteristics of the cutting material (Fig. 1), it should be noted that at high cutting speed and low feed rate, materials with high hardness and low strength [13, 14] can be used. These properties are inherent in ceramic materials. At great cutting depths, high mechanical strength is required, possessed by hard alloys [15]. This reduces the cutting speed. In addition, hard alloys have the optimal set of necessary properties for the cutting tool, which can be the benchmark both in structure and properties when designing a new cutting material.

Devising highly efficient tool ceramic materials is a relevant task of our time as it increases the productivity of machining, as well as the wear resistance and quality of the finished parts. In addition, it contributes to expanding the scope of application of tool materials by eliminating the costly grinding processes involving diamond abrasive wheels.

2. Literature review and problem statement

Great attention is paid to issues related to improving the mechanical properties of tool ceramics, producing tool materials based on chromium oxide, and determining patterns of influence of impurities, in particular aluminum nitride, on the structure and properties of tool materials.

Study [16] reports the development of a cutting tool alloyed with zirconium oxide of aluminum oxide with the addition of chromium. Its design involved a solid state process in which aluminum oxide powders (Al_2O_3), zirconium oxide (ZrO_2), and chromium oxide (Cr_2O_3) were processed in a ball mill. Compaction was carried out by cold isostatic pressing, sintering – at a steady temperature of $1,400^\circ\text{C}$ with a soaking time of 9 hours. The manufactured cutting tool was able to reach a service life of 225 s at a cutting speed of 200 m/min and a feed rate of 0.15 mm/rpm. However, at higher cutting speeds, the designed tool failed to operate; the wear mechanisms of manufactured cutting tools were not fully investigated.

In [17], the study focused on the analysis of friction and wear of ceramic cutting tools made from Al_2O_3 , ZrO_2 , and Cr_2O_3 . The tool was manufactured at machine AISI 1045. In that case, it was possible to increase the tool's service life by 51 % compared to $\text{Al}_2\text{O}_3\text{-ZrO}_2$ and an improvement of almost 800 % compared to Al_2O_3 . The addition of Cr_2O_3 enhanced the growth of Al_2O_3 grain, which contributed to better particle compaction and made it possible to obtain higher density, bending strength, and hardness. However, there remain unresolved issues related to the dependence of the microstructure of ceramic compacts obtained from $\text{Al}_2\text{O}_3\text{-ZrO}_2\text{-Cr}_2\text{O}_3$ with a mixing coefficient of 80–20–0.6 wt % on the tetragonal-monoclinic transitions.

Paper [18] investigated the wear of the cutting tool $\text{ZTA-TiO}_2\text{-Cr}_2\text{O}_3$ and the roughness of the machined surface of stainless steel 316L. The experiments were carried out at cutting speeds from 314 to 455 m/min, a feed rate from 0.1 to 0.15 mm/rev, and a cutting depth of 0.2 mm. For the lathe operation, the experiment made use of a lathe machine with numerical control. In addition, an optical microscope was used to analyze the side wear and the wear of craters, while the area of chips was observed using scanning electron microscopy. The lowest obtained values of the side wear, the wear of craters, and surface roughness were 0.044 mm, 0.45 mm^2 , $0.50\text{ }\mu\text{m}$, respectively, at the highest cutting speed of 455 m/min and the highest feed rate of 0.15 mm/rev. The limitation of the cited study is that the patterns of influence of impurities on the mechanical and operational properties of the resulting ceramic cutting tool, tempered on the basis of $\text{ZTA-TiO}_2\text{-Cr}_2\text{O}_3$, were not fully considered.

The authors of work [19], in order to improve the physical and mechanical properties of ceramics, considered the peculiarities of the formation of the microstructure of composites based on zirconium dioxide nanopowders, chemically synthesized using the method of decomposition of fluoride salts. It was established that reducing the porosity of nanopowders in the process of sintering is the key task on the way to the formation of high-density materials. It has been shown that an increase in the content of aluminum oxide nano additives leads to an increase in the strength and crack resistance of samples by simultaneously curbing the abnormal growth of grains and forming a smaller structure with a high tetragonal phase content. The limitation of the cited work is that

thermogravimetric studies were not carried out in full when sintering with various additives. In addition, not all samples were tested for the mechanical strength of the material, the mechanical properties were not fully compared with known world manufacturers of such materials.

Paper [20] proposes a method for quantifying the effect of alloy oxide on the coexistence of microstructure phases, the mobility of non-polarized ceramics charge carriers alloyed by different amounts of Fe_2O_3 and Cr_2O_3 . The measurement of electrical properties has shown that the doping of chromium and iron oxide contributes to the development of the tetragonal structural phase and leads to the transformation of the rhombohedral structure into a cubic shape. Chromium oxide is faster at driving the mobility of charge carriers of non-polarized material than iron oxide. Moreover, the addition of both chromium oxides and iron oxides contributes to an increase in the size of the tetragonal phase crystal. On the other hand, the size of the rhombohedral phase crystals increases due to the addition of iron oxide and decreases when alloying with chromium oxide. However, there remain unresolved issues related to determination the influence of the structural arrangement of composites based on chromium oxide on wear resistance. In addition, correlation bonds of thermomechanical properties were not considered.

In [21], the residues of the metallurgical industry, rich in Cr(III), were used for the synthesis of ceramic pigments. Cr_2O_3 chromium oxide was successfully separated from chromium waste by washing to extract soluble salts and pyrolysis up to 1,000 °C to decompose hydrated oxides, remove organic traces, and finally obtain appropriate oxides. Cr(III) oxide is accompanied mainly by Al(III) oxide and other insignificant impurities compatible with the composition of white ceramic raw materials. Thus, the chemical composition for the synthesis of ceramic pigments was obtained. The coatings had a homogeneous microstructure, without surface defects. The leaching test confirmed the assumption that vitreous dangerous chromium stabilizes well in vitreous matrices. In this way, ceramic technology contributes to inertization of this hazardous waste, destruction of the organic matter, reduction of the volume of wastes and its transformation into a useful material, with potential for commercial purposes. The limitation of the cited study is that the method for preparing the material used in the cited work is expensive. In addition, no comparative analysis of the quality of the resulting surface of ceramic material with known world analogs was carried out.

Paper [22] analyzed and compared the advantages and disadvantages of technologies and processes used to determine the most appropriate methods for designing ceramic cutting tools. The latest improvements in materials for ceramic cutting tools are considered. It has been shown that the choice of ceramic cutting tools is a rather complicated process, which should take into consideration a series of important factors. However, the cited paper does not fully take into account the chemical composition of the studied materials and structural transformations in them at friction. The wear resistance criteria discussed can be used for limited operating conditions and individual groups of materials.

The authors of [23] reported a study aimed at understanding the interphase tribological behavior when different types of tools are used for machining soft steel (MS) and high-chromium stainless steel (ST). The results show that fast-cutting steel (HSS) suffers severe abrasive wear at MS and causes serious ST sticking problems. It was established

that the oxide scale on the surface of metal slip contributes to wear resistance. However, for high-chromium stainless steels, oxidation is significantly inhibited by the formation of a protective layer of chromium (Cr_2O_3 or $(\text{Fe}_{1-x}\text{Cr}_x)_2\text{O}_3$), which is self-repaired at high temperatures. This layer can prevent iron diffusion outwards and oxygen diffusion inside, leading to several issues during hot molding, such as uneven tool wear and sticking phenomenon.

The review of studies has shown that chromium oxide with the additives of ultra-dispersed powder of aluminum nitride is a promising material for use in tools with improved cutting and anti-wear properties. When designing a cutting tool, the focus is on the investigation of the mechanical characteristics of the material, especially crack resistance and hardness. When conducting friction and wear tests, the impact of the structural structure of composites based on chromium oxide on wear resistance is mostly not taken into consideration. In most studies, no correlation bonds between the thermomechanical and tribological properties were established. Almost unattended were those issues that relate to the compatibility and mutual impact of the tribosystem “ceramic composite – metal” on the friction processes in the contact zone.

Thus, the task of determining the effect of ultra-dispersed additives of aluminum nitride on the structure and physical-mechanical properties of tool ceramics needs to be addressed. In addition, designing effective cutting tools, improving the quality of machined surfaces of high-alloy steels, using modern methods for the formation and sintering of nanopowders create new opportunities to produce composite materials with high operational capabilities.

3. The study materials and methods

The purpose of this study is to determine the effect of ultra-dispersed additives of aluminum nitride on the structure and physical-mechanical properties of tool ceramics based on chromium oxide, which could make it possible to produce tool material with high performance properties.

To accomplish the aim, the following tasks have been set:

- to investigate the microstructure of composite materials based on chromium oxide under hot pressing;
- to determine the regularities of influence of aluminum nitride additives on the structure and physical-mechanical properties of tool materials based on the synthesized chromium oxide nanopowder;
- to compare the quality of the machined surface of the high-strength alloyed steel of the designed tool material with the best imported analogs.

4. The study materials and methods

We used the following powders manufactured by Sigma Aldrich Chemie GmbH (Germany): Cr_2O_3 the size of 1–3 μm , and AlN A200 the size of 0.7–1.8 μm .

The mixtures were mixed in agate drums in a planetary mill with a rotational speed of 5 m/s for 30–40 minutes.

Ethyl alcohol was used as a mixing medium.

The ratio of the starting mixture, alcohol, and mixing balls was, respectively, 2:1:1. After mixing, the mixtures were dried and rubbed through sieve No. 0064. The mixtures of powders “chromium oxide – aluminum”, “chromium

oxide – aluminum nitride” were subjected to briquetting in steel molds in a vacuum. To study the structure formation and properties in these powders at high temperatures, briquetted samples were subjected to hot pressing in a vacuum at a pressure of 30 MPa at the installation for electric sintering.

Some physical and mechanical properties of the obtained composites $(\text{Cr, Al})_2\text{O}_3\text{-CrN}$ were determined according to the generally accepted procedures by using standard equipment [24, 25]. The bending strength limit was determined with the help of the MH-1 test machine on samples the size of $5 \times 5 \times 35$ mm when applying a concentrated force at a speed of 40 m/s; the number of samples – 5 pieces per pack.

The compression strength limit was determined at the UMN-10 test plant. Samples were polished to the purity specified by GOST 2789-73 to the size of $5 \times 5 \times 10$ mm; the number of samples – 5 pieces per one point.

The hardness of the obtained compositions was measured by the PMT-3 microhardness meter using instructions for optimal load values and the time of their action.

The crack resistance of materials was determined by identification involving the Vickers pyramid using carefully polished microsection according to the procedure proposed in [26].

The viscosity coefficient of destruction, characterizing the crack resistance of the sample, was determined from the following expression [27]:

$$K_{IC} = 0.016 \cdot \left(\frac{l}{a}\right)^{-0.5} \cdot \left(\frac{H_V}{E \cdot F}\right)^{-0.4} \cdot \frac{H_V \cdot a^{0.5}}{F}, \quad (1)$$

where H_V is the micro-hardness, GPa; E is the Young module, GPa; F – a constant, $F \approx 3$; l is the length of the crack from the angle of the Vickers pyramid, m; a is the half-band fingerprint of the Vickers pyramid, the average distance from the center of the imprint to the end of the crack, m.

Apparent density, relative density, and porosity were determined according to the methodology set by GOST 20018-74.

X-ray images of powder samples were acquired from the diffractometers “Dron-3.0” and URS-50 in Cu_α -radiation with a Ni-filter.

The acquisition of fractograms of breaking surfaces was carried out at a raster electron microscope.

Micro-X-ray spectral analysis was carried out at the Camscan raster electron microscope, which makes it possible to determine the qualitative, semi-quantitative, and quantitative distribution of elements at certain points of the surface.

The qualitative chemical analysis along the line was carried out with the help of ILink-860 system; the quantitative chemical analysis – employing the ZAF-4 software. In semi-qualitative analysis, computer simulation was used.

When processing the results of experiments, the methods of mathematical statistics were used [28, 29].

Metallographic studies of the structure of the obtained materials and their photographing were carried out at the metallographic microscopes MIM-8 “Neophot-2” in reflected light with magnification from 300 to 1,000 times.

To obtain high-quality micro sections, we machined the sample plane at the universal-sharpening machine ZB456. In this case, the sample was fixed in a special mold and consistently polished with diamond wheels with a grain size of 60/40, 20/14, 7/5, 3/2 μm using a cooling water-based liquid.

The thermal conductivity coefficient was determined at room temperature on samples of a rectangular shape of $15 \times 15 \times 1$ mm at the device for measuring the thermal conductivity NT-3 MHTI.

Tempered steel 13HV (HRC 57..60) was used as the material for machining.

The roughness of the machined surface was investigated at the special device KEYENCE (Japan) shown in Fig. 2.



Fig. 2. Device for measuring roughness and quality of the machined surface

The KEYENCE device (Fig. 2) makes it possible to determine the quality of the machined surface of the part for several indicators at once. With its help, we determined the profile of the machined surface, roughness parameters, as well as the topography of the surface in general, based on the distribution of heterogeneities in the surface layer of the samples studied.

The tribological tests of sintered samples were carried out at an ambient temperature of 25 °C and relative humidity of 50 % at the Microngamma device. The structural diagram of the device is given in [30]; in the test mode of pin-on-disk at reciprocating friction – in [31]; at the friction machine in the test mode of ball-micro section (calo-test) – in [32].

The surfaces of the samples were pre-polished using SiC materials up to 5 μm and an oxide suspension based on colloidal silicon dioxide particles the size of 100 nm.

Tests involving the reciprocating friction of sintered samples were carried out by a diamond conical indenter with a rounding radius at a top of 50 μm at a load of 500 mN and a slip speed of 20 $\mu\text{m/s}$.

The wear of friction paths was measured at the contactless 3D Micron-alpha interference profiler, consisting of an optical electron unit and a system of micromirrors [33, 34]. It registers surface irregularities at nanometric accuracy, which makes it possible to measure the volume of the friction path.

Based on the acquired experimental data, we determined the wear rate from the following expression [35]:

$$I = \frac{V}{P_N \cdot L \cdot n}, \quad (2)$$

where V is the volume of the friction path (the loss of sample wear volume), μm^3 ;

P_N is the applied normal force, N;

L is the path length (the distance covered by the indenter per one cycle), μm ;

n is the number of cycles.

The tests met international standards ASTM G99-959, DIN 50324, and ISO 20808.

5. Results of studying the effect of ultra-dispersed additives of aluminum nitride on the structure and properties of ceramics

5.1. The microstructure of composite materials based on chromium oxide under hot pressing

Designing new materials with predefined properties is perhaps the most important issue and the task of modern materials science [36]. The cutting Al₂O₃-based ceramics, strengthened with 10...20 wt % of silicon carbide fibers, ensure high purity of the machined surface [37, 38]. Silicon carbide strengthening makes it possible to apply this material when machining heat-resistant nickel alloys with cutting speeds exceeding 200 m/min and a feed rate of 0.16 mm/rev. The high strength and viscosity of destruction make it possible to effectively use such ceramics for machining cast iron. However, in terms of ensuring the quality of the machined surface, of interest is the Cr₂O₃-based cutting ceramics. This material has good abrasive properties and is used as polishing pastes [39, 40]. Chromium oxide, being a refractive material with a high melting point and oxidation resistance, is widely used to produce ceramics. In addition, Cr₂O₃ is a carrier for catalysts or is part of them, which makes it possible to use such catalysts up to 1,000 °C, without a noticeable change in composition [41]. Table 1 gives the comparison of the physical and mechanical properties of chromium and aluminum oxides.

Table 1 shows that the Cr₂O₃ material has a higher hardness and melting point than Al₂O₃.

Chromium forms a series of oxygen compounds CrO, Cr₂O₃, CrO₃ whose physicochemical nature, the properties and mutual transitions are complex and diverse. Between these oxides, there are several intermediate oxygen compounds whose compositions have not yet been precisely established. The higher chromium oxide CrO₃ has a low melting point (about 195 °C) and, when heated, decomposes into a series of intermediate oxides. Chromium oxide CrO is unstable in the air and quickly turns into a stronger oxide Cr₂O₃. The Cr-O state diagram is shown in Fig. 3.

The Cr-O state diagram (Fig. 3) demonstrates that at temperatures below 1,600 °C there is a two-phase region Cr+Cr₂O₃, and, within the temperature range of 1,600–1,660 °C, there is a two-phase region Cr+Cr₃O₄. The Cr+Cr₃O₄ materials (31.58 wt %) have a region of non-mixing between 780 and 1,300 °C.

Chromium oxide Cr₂O₃ is industrially produced from chromite ore by obtaining an intermediate compound of sodium bichromate, as well as direct oxidation of chromium. Cr₂O₃ has a rhombohedral lattice, the type of Al₂O₃, with the following parameters of the elementary cell: *a*=4.950 Å, *c*=13.665 Å, *c/a*=2.761 at 20 °C.

Chromium oxide begins to decompose at a temperature of 1,257 °C, at 1,200 °C – with the formation of Cr₃O₄. It is likely that the reasons for the discrepancy in dissociation temperature are related to the private reduction of Cr³⁺ to Cr²⁺.

The caloric value of chromium oxide formation at 2,516 °C is equal to 4,691.4 kJ/mol. Specific electric conductivity at 20 °C ranges between 3.4·10⁻⁶ and 1.2·10⁻⁴ Ohm⁻¹·m⁻¹.

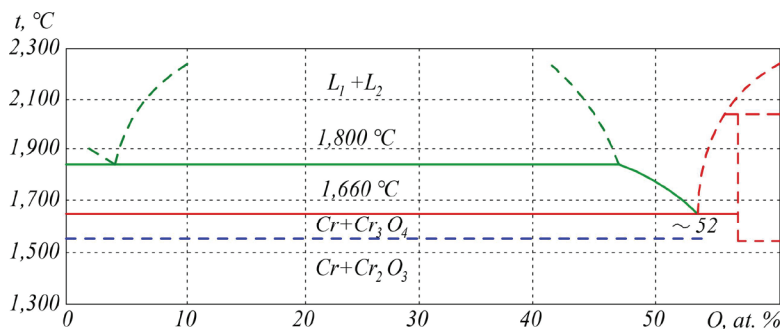


Fig. 3. The Cr-O state diagram: L₁ – Cr₂O₃ liquid state; L₂ – Cr liquid state

Table 1

Physical and mechanical properties of chromium and aluminum oxides

Material	γ, g/cm ³	T _{mel} , K	HV	σ _b , N/m ²	σ _{st} , MN/m ²	E, GN/m ²	λ, W/(m·K)	ρ, Ohm·m
Al ₂ O ₃	3.8–3.9	2,320	2,800	330	3,000	360	20	10 ¹⁴
Cr ₂ O ₃	5.21	2,573	2,915	300	2,900	284	19	10 ⁵

Chromium oxide is characterized by exceptional chemical inertia, which is a great advantage in the processing of various alloys. The oxygen and temperature limit of stability is determined from the following dissociation reaction [42]:



The dissociation pressure P_{O₂}^{dis}, MPa, and dissociation temperature are related via the following equation [43]:

$$\lg P_{O_2}^{dis} = 0.1 \cdot \left[7.16 - \frac{3,579}{t} \right] \tag{4}$$

Dissociation negatively affects the sintering and hot pressing of chromium oxide. It is known to limit the oxygen content in the gas environment, with a decrease in which the number of oxygen vacancies in the oxide increases, so the sintering occurs better. The partial pressure of oxygen P_{O₂}^{dis}, over the oxide is [44]:

$$P_{O_2}^{dis} = K^{2/3} [Cr]^{-4/3} \tag{5}$$

where K is the equilibrium constant.

The creation of dense and high-strength chromium oxide is complicated by the decomposition and evaporation of Cr₂O₃, the result of which is microporosity that reduces the mechanical characteristics [45]. The main gaseous product on the surface of chromium oxide is chromium anhydride Cr₂O₃, so weight loss occurs due to the following reaction:



Dissociation of chromium oxide can be damped by rapid compaction and the creation of closed porosity by applying high pressure. One of the promising ways to obtain dense articles from Cr₂O₃ is to introduce additives that actively interact with the oxide and thereby prevent its dissociation. One of these materials is ultra-dispersed aluminum nitride powder. Aluminum nitride has high enough thermal conductivity, so its addition to chromium oxide helps increase the thermal conductivity of the tool material in general [46].

In addition, the comprehensive study of dielectric characteristics in wide ranges of frequencies, electrical resistance, and thermal conductivity of AlN-based composites makes these materials promising and competitive [47].

Designing tool materials with the high wear resistance, without the use of lubricants, and high quality of the machined surface, low roughness, which could replace some technological processes of grinding with fine turning, is a relevant task.

5.2. The effect of aluminum nitride additives on the structure and properties of materials based on chromium oxide

In order to maximize the compaction of the material at the initial stage to reduce the temperature and time of hot pressing, the mixtures “chromium oxide – aluminum nitride” were pre-pressed in steel molds. Fig. 4 demonstrates that the densest samples could be obtained when pressing in a vacuum. This is due to the fact that the air is pressed (compressed) and its pressure can reach 10 MPa [48].

Subsequently, after removing the load, compressed air expands and leads not only to an increase in porosity but also, in some cases, to the stratification of the sample. The comparison of the estimation and experimental porosity values in the case of pressing in the air revealed that they are approximately the same.

After cold pressing in a vacuum, the samples were installed in graphite molds and subjected to hot pressing. The hot pressing was carried out at temperatures of 1,500–1,700 °C under a pressure of 15–30 MPa. The kinetics of hot pressing the mixture Cr_2O_3 – 15 wt % AlN are shown in Fig. 5.

Fig. 5 shows that increasing pressure and temperature increases relative density, and accordingly, decreases the porosity. The densest samples can be obtained at a pressure of 30 MPa and a hot-pressing time of 4–6 minutes.

The lower temperature limit of hot pressing of 1,500 °C was chosen on the basis of the differential thermal analysis of the mixture Cr_2O_3 – 15 wt % AlN (Fig. 6), according to which the interaction in this system begins at a temperature of 1,435 °C.

The thermodynamic calculations of the interaction of chromium oxide with aluminum nitride showed that the interaction between them begins at a temperature of 1,300 °C. Table 2 gives the equilibrium content of the components formed during the reaction process. Calculations were carried out according to a specially developed program for ideal multicomponent heterogeneous systems [49].

Table 2 demonstrates that with the hot pressing in the air, the $(\text{Cr}, \text{Al})_2\text{O}_3$, Cr_2N , CrN , Cr compounds are formed. Unlike hot pressing in the air, no CrN and Cr_2N compounds are formed in a vacuum. As the temperature rises, the Al_2O_3 content in solid solution is maximum at a temperature of 1,700 °C in the case of hot pressing in the air; in a vacuum,

the content of Al_2O_3 remains unchanged throughout the temperature range of 1,300–1,700 °C.

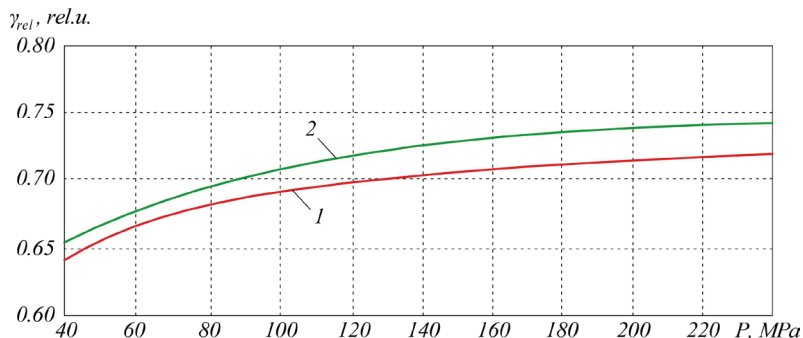


Fig. 4. Dependence of the relative density on the pressure during cold pressing: 1 – in the air; 2 – in a vacuum

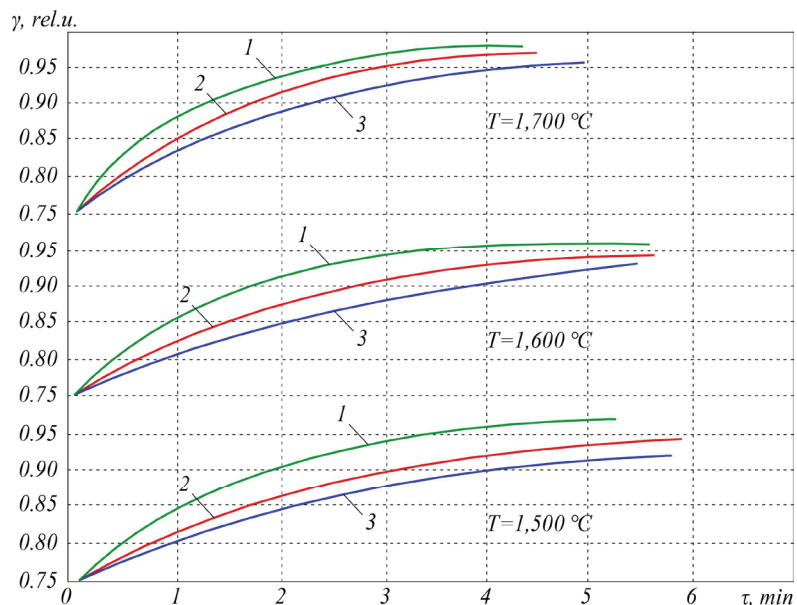


Fig. 5. Dependence of the relative density on the temperature and time of hot pressing for the mixture Cr_2O_3 – 15 wt % AlN: 1 – at a pressure of 30 MPa; 2 – at a pressure of 20 MPa; 3 – at a pressure of 15 MPa

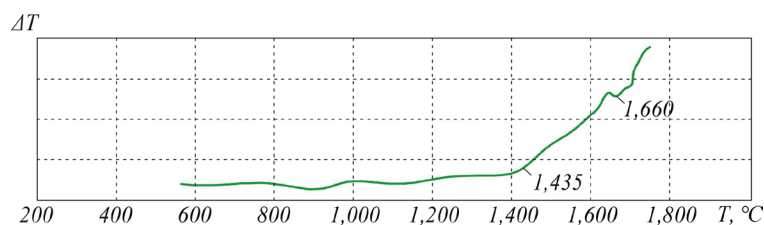


Fig. 6. Heating thermogram of the Cr_2O_3 – 15 wt % AlN mixture in argon

X-ray phase analysis of the samples, hot-pressed in the air at a temperature of 1,600 °C, confirmed the presence of $(\text{Cr}, \text{Al})_2\text{O}_3$, Cr_2N , CrN phases.

Fig. 7 shows the structure of the composite obtained by hot pressing in the air from the mixture of Cr_2O_3 – 15 wt % AlN at different temperatures.

At a temperature of 1,500 °C, the structure consists of gray and white phases, and, at 1,700 °C, dark areas are visible, which is likely the compound $\text{Cr}_{1.36}\text{Al}_{0.64}\text{O}_3$, judging by the data of chemical analysis (Tables 3, 4).

Quantitative analysis (Table 4) reveals that at 1,700 °C, a large amount of aluminum is contained in the dark oxide phase of the composite. It is a solid solution of $\text{Cr}_{1.4}\text{Al}_{0.6}\text{O}_3$. In

the gray phase, the content of aluminum is much smaller, and it mainly consists of chromium oxide Cr_2O_3 . The structure of the composite depends both on the temperature and the time of hot pressing. With an increase in hot pressing time to 30 min, the size of individual grains reaches $10\ \mu\text{m}$ (Fig. 8).

Table 2

Data of the thermodynamic calculation of equilibrium content of components in a composite with the output mixture $\text{Cr}_2\text{O}_3 - 15\ \text{wt}\ \% \text{ AlN}$, mol/kg

$T, ^\circ\text{C}$	Component	P, MPa		
		30	0.0098	0.0098
1,300	Cr_2O_3	0.4827	0.9994	0.9994
	Al_2O_3	0.0069	0.0002	0.0002
	CrN	0.4979	–	–
	Cr_2N	–	–	–
	Cr	0.0009	0.0002	0.0002
1,400	Cr_2O_3	6.0030	0.9994	0.9994
	Al_2O_3	0.6471	0.0002	0.0002
	CrN	–	–	–
	Cr_2N	0.0120	–	–
	Cr	0.0003	0.0002	0.0002
1,500	Cr_2O_3	3.4827	0.9994	6.5756
	Al_2O_3	0.4768	0.0024	0.0025
	CrN	–	–	–
	Cr_2N	0.0001	–	–
	Cr	0.0395	0.0002	0.0025
1,600	Cr_2O_3	4.7493	0.9994	0.9994
	Al_2O_3	0.3584	0.0002	0.0002
	CrN	0.0013	–	–
	Cr_2N	0.2990	–	–
	Cr	0.0001	0.0002	0.0002
1,700	Cr_2O_3	7.1539	0.9994	0.9994
	Al_2O_3	0.5264	0.0002	0.0002
	CrN	0.0034	–	–
	Cr_2N	0.0007	–	–
	Cr	0.0002	0.0002	0.0002

Table 3

The result of quantitative analysis of the distribution of Cr, Al, O in the sample, hot-pressed in the air, from a mixture of $\text{Cr}_2\text{O}_3 - 15\ \text{wt}\ \% \text{ AlN}$ at $T=1,500\ ^\circ\text{C}$

Hot pressing parameters	Elemental content, wt %					
	Light phase, point 1			Grey phase, point 2		
	Cr	Al	O	Cr	Al	O
$P=30\ \text{MPa};$ $T=1,500\ ^\circ\text{C};$ $\tau=6 \cdot 10^2\ \text{s}$	98.529	0.101	0.292	89.311	6.286	3.906

The result of quantitative analysis of the distribution of Cr, Al, O in the sample, hot-pressed in the air, from a mixture of $\text{Cr}_2\text{O}_3 - 15\ \text{wt}\ \% \text{ AlN}$ at $T=1,700\ ^\circ\text{C}$

Hot pressing parameters	Elemental content, wt %								
	Light phase, point 1			Grey phase, point 2			Dark phase, point 3		
	Cr	Al	O	Cr	Al	O	Cr	Al	O
$P=30\ \text{MPa};$ $T=1,700\ ^\circ\text{C};$ $\tau=6 \cdot 10^2\ \text{s}$	96.479	1.729	1.026	81.082	13.172	5.698	71.464	23.735	4.804

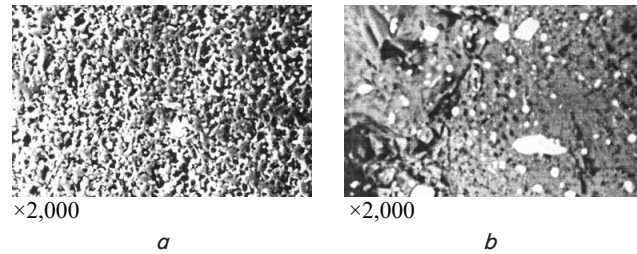


Fig. 7. The structure of composite material $\text{Cr}_2\text{O}_3 - 15\ \text{wt}\ \% \text{ AlN}$, hot-pressed in the air under the following conditions: $a - P=30\ \text{MPa}, T=1,500\ ^\circ\text{C}, \tau=10\ \text{min}; b - P=30\ \text{MPa}, T=1,700\ ^\circ\text{C}, \tau=10\ \text{min}$

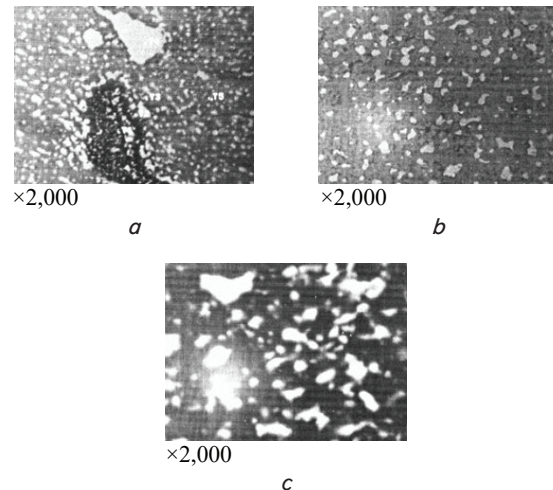


Fig. 8. The structure of composites $\text{Cr}_2\text{O}_3 - 15\ \text{wt}\ \% \text{ AlN}$, hot-pressed in the air at $P=30\ \text{MPa}, T=1,500\ ^\circ\text{C}$, during the time: $a - \tau=10\ \text{min}; b - \tau=15\ \text{min}; c - \tau=30\ \text{min}$

Fig. 8 shows that with hot pressing, zones with high aluminum content in a solid solution are formed in some areas of the composite. The quantitative composition of elements at individual points of samples is given in Table 5.

Table 5

The result of quantitative analysis of the distribution of Cr, Al, O in the samples, hot-pressed in the air, from a mixture of $\text{Cr}_2\text{O}_3 - 15\ \text{wt}\ \% \text{ AlN}$ at $P=30\ \text{MPa}; T=1,700\ ^\circ\text{C}; \tau=6 \cdot 10^2\ \text{s}$

Elemental content, wt %					
Point 1			Point 2		
Cr	Al	O	Cr	Al	O
56.499	41.036	2.034	55.382	40.606	3.604
Elemental content, wt %					
Point 3			Point 4		
Cr	Al	O	Cr	Al	O
74.709	21.777	3.457	95.867	1.863	0.882

Table 6

As the time of hot pressing increases, the quantitative composition of the elements changes [50, 51]. The amount of aluminum in the light phase increases and its content decreases in the gray phase (Table 6).

Fig. 8, 9 show how the structure of the $\text{Cr}_2\text{O}_3 - 15\ \text{wt}\ \% \text{ AlN}$ composite changes at hot pressing dependence on the temperature and time. With increasing the time of hot-pressing temperature, chromium grains increase. For instance, at the temperature $T=1,500\ ^\circ\text{C}$ and an aging time of 10 minutes, the size of chromium grains is $1\ \mu\text{m}$; with an increase in the time to 30 min-

utes, their size reaches 3–4 μm. At a temperature of 1,700 °C, the average size of chromium grains is 3–5 μm at an aging time of 10 minutes, and 5–8 μm at an aging time of 20 minutes. There are also separate inclusions the size of 10–12 μm.

Table 7 gives data on the chemical analysis that demonstrate that when the temperature rises, the content of aluminum and oxygen in the light phase decreases, while increasing the content of aluminum in the gray phase. X-ray microanalysis and X-ray phase analysis showed that the solid solution (Cr, Al)₂O₃, the Cr₂N, CrN compounds, and pure chromium are formed in the samples obtained by the hot pressing in the temperature range of 1,500–1,700 °C. This is also confirmed by thermodynamic calculations given in Table 2.

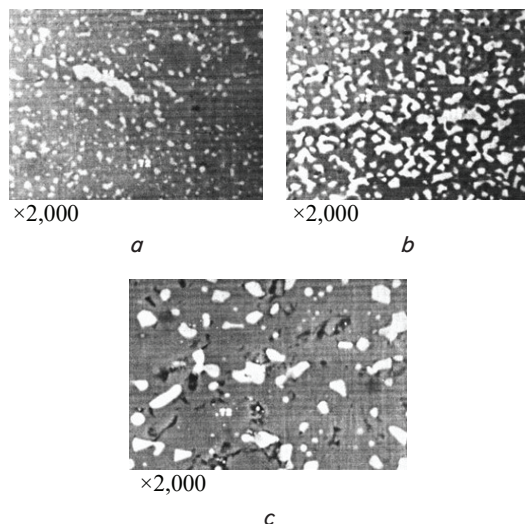


Fig. 9. The structure of Cr₂O₃ – 15 wt % AlN composites, hot-pressed in a vacuum: a – P=30 MPa, T=1,600 °C, τ=10 min; b – P=30 MPa, T=1,700 °C, τ=10 min; c – P=30 MPa, T=1,700 °C, τ=20 min

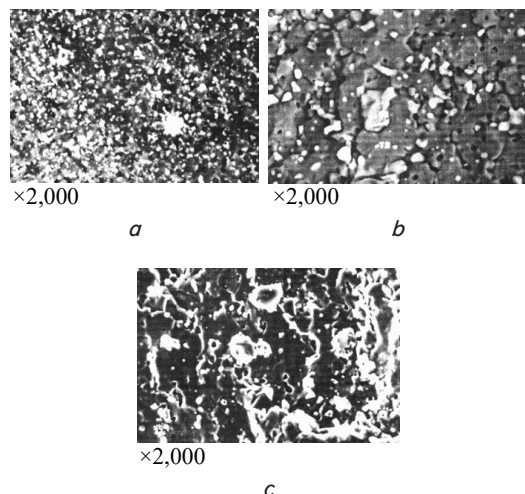


Fig. 10. Structure and fractogram of the composite Cr₂O₃ – 15 wt % AlN, obtained by hot pressing in a vacuum at P=30 MPa, τ=10 min, at temperature: a – T=1,500 °C; b – T=1,600 °C; c – T=1,700 °C

Fig. 11, a shows the distribution of chromium and aluminum by the area of the model sample, hot-pressed in the air

at a temperature of 1,500 °C and an aging time of 10 minutes. Fig. 11, b demonstrates that a transition zone 15 μm wide is formed between Cr₂O₃.

A similar pattern is revealed in the case of hot pressing at a temperature of 1,600 °C (Fig. 12).

Table 6

The result of quantitative analysis of the distribution of Cr, Al, O in the samples, hot-pressed in the air, from a mixture of Cr₂O₃ – 15 wt % AlN

Sample No.	Hot pressing parameters: P=30 MPa; T=1,700 °C	Elemental content, wt %					
		Light phase, point 1			Gray phase, point 2		
		Cr	Al	O	Cr	Al	O
1	τ=6·10 ² s	98.529	0.101	2.292	89.341	6.286	3.906
2	τ=9·10 ² s	99.249	0.109	0.642	89.653	6.028	4.212
3	τ=12·10 ² s	99.115	0.117	0.728	90.066	5.737	4.950
4	τ=18·10 ² s	99.082	0.126	0.792	89.735	5.267	4.998

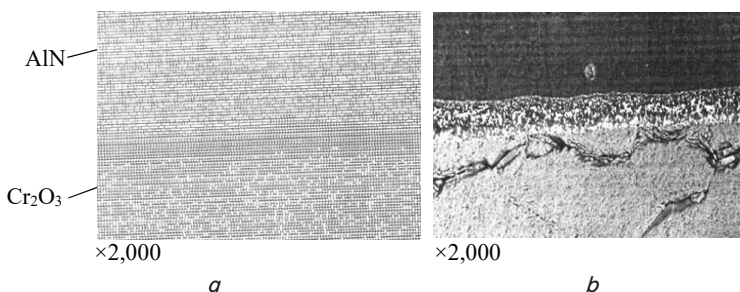


Fig. 11. Study of the sample obtained by hot pressing at P=30 MPa, T=1,500 °C, τ=10 min: a – distribution of chromium and aluminum by the area of the model sample; b – formation of a transition zone 15 μm width

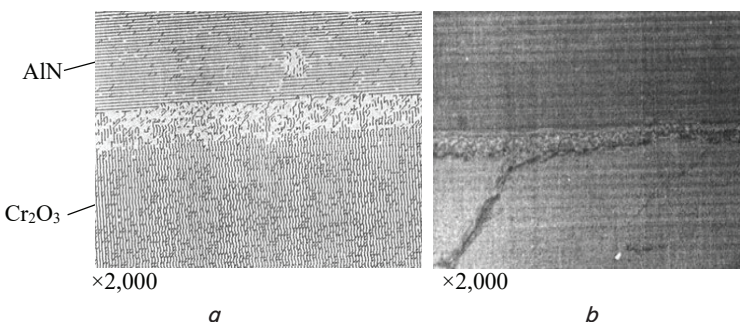


Fig. 12. Study of the sample obtained by hot pressing at P=30 MPa, T=1,600 °C, τ=10 min: a – distribution of chromium and aluminum by the area of the model sample; b – formation of a transition zone

Table 7

The result of quantitative analysis of the distribution of Cr, Al, O in the hot-pressed samples from the mixture of Cr₂O₃ – 15 wt % AlN (Fig. 10)

Sample No.	Hot pressing parameters: P=30 MPa; τ=12·10 ² s	Elemental content, wt %					
		Light phase, point 1			Gray phase, point 2		
		Cr	Al	O	Cr	Al	O
1	T=1,500 °C	94.596	3.924	1.381	84.884	10.852	4.037
2	T=1,600 °C	96.658	2.138	0.613	84.777	12.010	3.193
3	T=1,700 °C	98.723	0.121	0.460	84.896	12.117	2.857

The transition zone is a solid solution of (Cr, Al)₂O₃. The distribution of chromium and aluminum along the line of passing the scanning beam of the microscope on the model sample obtained by hot pressing at P=30 MPa, T=1,600 °C, τ=10 min, is shown in Fig. 13.

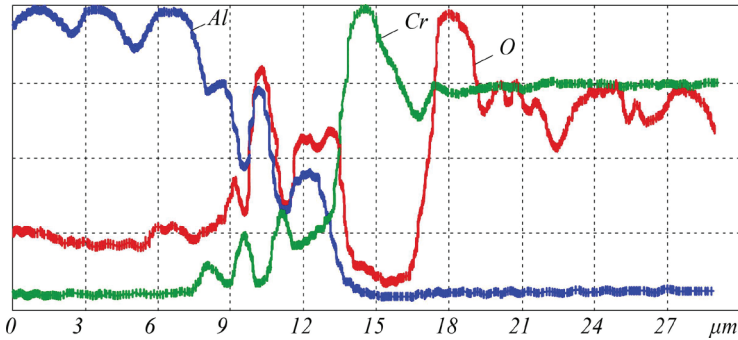
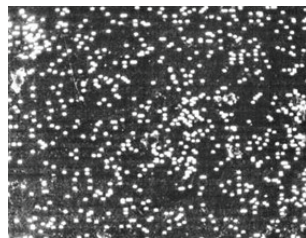


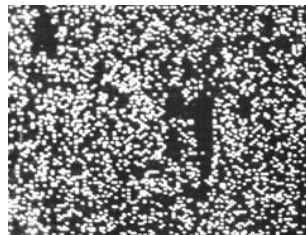
Fig. 13. Distribution of chromium and aluminum by the area of the model sample obtained by hot pressing at $P=30$ MPa, $T=1,600$ °C, $\tau=10$ min

The distribution of elements (aluminum and chromium) by the area of the entire surface of the sample obtained by hot pressing from $Cr_2O_3 - 15$ wt % at $P=30$ MPa, $T=1,600$ °C, $\tau=10$ min, is shown in Fig. 14.



×2,000

a



×2,000

b

Fig. 14. Distribution of elements by the area of the entire surface of the sample obtained by hot pressing from $Cr_2O_3 - 15$ wt % AlN at $P=30$ MPa, $T=1,600$ °C, $\tau=10$ min: a – aluminum distribution; b – chromium distribution

Fig. 14 demonstrates that aluminum and chrome are distributed evenly over the total area of the sample.

5.3. Comparing the quality of the machined surface of high-strength steel by the developed tool material with imported analogs

Fig. 15 shows the process of machining the tempered steel 13HV.



Fig. 15. Machining the tempered steel 13HV (HRC 57...60)

Table 8 gives the comparative characteristics of the assessment of the quality of the surface machining of tempered steel by standard cutting plates manufactured by Sandvik Coromant (Sweden) and plates from the material developed on the basis of chromium oxide.

Table 8

Characteristics for estimating the machining quality of the surface of tempered steel

Material name	Sandvik Coromant 650	Developed material
Starting surface		
Surface with limited scale		
Material ratio curve		
Autocorrelation function		
Angle spectrum		

Our study of the quality of the machined surface compared with the cutting plates made by Sandvik Coromant (Sweden) has shown that the quality of the machined tempered steel when using plates from the material developed on the basis of chromium oxide is higher than that of standard imported plates. It should be noted that the introduction of aluminum nitride makes it possible to increase the thermal conductivity of chromium oxide to 35 W/(m·K). This factor has a positive effect on the removal of heat from the cutting zone, which also affects the quality of the machined surface since no lubricating-cooling liquids were used.

Tribological comparative studies have shown that the wear rate of the developed material based on $\text{Cr}_2\text{O}_3 - 15 \text{ wt } \% \text{ AlN}$ was $10.04 \cdot 10^{-6} \text{ mm}^3 \cdot \text{N}^{-1}$. For a similar type of Sandvik Coromant 650 cutting plate, the wear speed was $12.10 \cdot 10^{-6} \text{ mm}^3 \cdot \text{N}^{-1}$. This indicates the high wear resistance of the developed ceramic tool material based on chromium oxide with the additives of ultra-dispersed aluminum nitride powder.

6. Discussion of results of studying the effect of aluminum nitride additives on the structure and properties of ceramics

Our study has shown that in terms of ensuring the quality of the machined surface, the Cr_2O_3 -based cutting ceramics are of interest. Cr_2O_3 material has a higher hardness and melting point than Al_2O_3 (Table 1). At temperatures below 1,600 °C, there is a two-phase region $\text{Cr} + \text{Cr}_2\text{O}_3$, and, in the temperature range of 1,600–1,660 °C, there is a two-phase region $\text{Cr} + \text{Cr}_3\text{O}_4$ (Fig. 3). The creation of a dense and high-strength chromium oxide is complicated by the decomposition and evaporation of Cr_2O_3 , as a result of which microporosity forms, which reduces mechanical characteristics. One of the ways to obtain dense articles from chromium oxide is to introduce an admixture of ultra-dispersed aluminum nitride powder, which actively interacts with oxide and thereby prevents its dissociation. The densest samples can be obtained at a pressure of 30 MPa and a hot-pressing time of 8–10 min when pressing in a vacuum (Fig. 4). As pressure and temperature increase, the relative density increases while porosity decreases accordingly (Fig. 5).

We have determined the equilibrium content of the components formed during the reaction of chromium oxide with aluminum nitride (Table 2), which begins at a temperature of 1,300 °C. The structure of the composite material obtained by hot pressing in the air from a mixture of $\text{Cr}_2\text{O}_3 - 15 \text{ wt } \% \text{ AlN}$ at different temperature values (Fig. 7) was determined. Quantitative analysis of the distribution of Cr, Al, O in the samples, hot-pressed in the air, from the mixture of $\text{Cr}_2\text{O}_3 - 15 \text{ wt } \% \text{ AlN}$ depending on the temperature and the time of hot pressing (Tables 5–7) was performed. X-ray microanalysis and X-ray phase analysis showed that in the samples obtained by hot pressing in the temperature range of 1,500–1,700 °C, the solid solution of the overcoat type $((\text{Cr}, \text{Al})_2\text{O}_3)$ is formed. This helps increase the strength and crack resistance of the material. The distribution of elements by the area of the model sample obtained by hot pressing showed that aluminum and chrome are distributed evenly over the entire area of the sample (Fig. 14).

Our study of cutting plates based on the resulting material demonstrated the high quality of the machined surface of tempered steel 13HV (Fig. 15). Ultra dispersed aluminum nitride powders increase the thermal conductivity of the

cutting material, thereby contributing to the improvement of the quality of the machined surface of tempered steel. In addition, comparing the quality of the machined surface with that machined by the Sandvik Coromant cutting plates showed that the quality of the tempered steel, machined with plates from the material developed on the basis of chromium oxide, is higher than that of standard imported plates. The developed tool material can be used for the fine turning of high-strength steels and cast irons without lubricants and coolants instead of grinding, which could significantly reduce the cost of machining. In particular, the material would be promising for machining a surfaced layer of railroad cars' wheelsets during repair work.

The limitation of the current study is that the operational properties of the proposed material have not been fully investigated, for example, wear resistance when machining various tempered steels. In addition, not all samples were tested for the mechanical strength of the material; the cutting properties were not compared in full with known world manufacturers of such materials.

In further studies, it would be advisable to achieve greater dispersion of chromium oxide grains. In addition, such modes of sintering should be optimized as the rate of increase in temperature with hot pressing, the aging time at the final temperature, an increase in the pressure applied to the material.

7. Conclusions

1. We have investigated the microstructure of composite materials based on chromium oxide under hot pressing. It is determined that the creation of dense and high-strength chromium oxide is complicated by the decomposition and evaporation of Cr_2O_3 , as a result of which microporosity is formed, which reduces mechanical characteristics. One of the promising ways to produce dense articles from Cr_2O_3 is to introduce additives that actively interact with the oxide and thereby prevent its dissociation. One of these materials is ultra-dispersed aluminum nitride powder.

2. The regularities of influence of aluminum nitride additives on the structure and physical-mechanical properties of tool materials based on the synthesized nanopowder of chromium oxide have been determined. Thus, the structure of the composite depends both on the temperature and time of hot pressing. With an increase in hot-pressing time to 30 min, the size of individual grains reaches 10 μm . At the same time, X-ray microanalysis and X-ray phase analysis showed that the solid solution of $(\text{Cr}, \text{Al})_2\text{O}_3$, the Cr_2N , CrN compounds, and pure chromium are formed in samples obtained by hot pressing in the temperature range of 1,500–1,700 °C.

3. We have compared the characteristics of the quality assessment of the machined surface of tempered steel when using standard cutting plates manufactured by Sandvik Coromant and plates from the material developed on the basis of chromium oxide. It is determined that the quality of the tempered steel machined with plates from the material developed on the basis of chromium oxide is higher than that of standard imported plates. In addition, the introduction of aluminum nitride prevents the destruction of chromium oxide during hot pressing due to reaction sintering and makes it possible to improve the strength and increase the thermal conductivity of the tool material.

Acknowledgments

The article was prepared as part of a study under the state budget topic “The Use of Non-traditional Methods of

Obtaining Nanopowders and Sintering in the Development of Modified Mullite-ZrO₂ Ceramics Resistant to Heat Shock” (State Registration Number 0121U109441) with the financial support of the Ministry of Education and Science of Ukraine.

References

1. Vovk, R. V., Hevorkian, E. S., Nerubatskyi, V. P., Prokopiv, M. M., Chyshkala, V. O., Melnyk, O. M. (2018). Novi keramichni kompozytsiyni materialy instrumentalnoho pryznachennia. Kharkiv: KhNU imeni V. N. Karazina, 200. Available at: <http://lib.kart.edu.ua/handle/123456789/5086>
2. Rizzo, A., Goel, S., Luisa Grilli, M., Iglesias, R., Jaworska, L., Lapkovskis, V. et. al. (2020). The Critical Raw Materials in Cutting Tools for Machining Applications: A Review. *Materials*, 13 (6), 1377. doi: <https://doi.org/10.3390/ma13061377>
3. Gevorkyan, E. S., Rucki, M., Kagramanyan, A. A., Nerubatskiy, V. P. (2019). Composite material for instrumental applications based on micro powder Al₂O₃ with additives nano-powder SiC. *International Journal of Refractory Metals and Hard Materials*, 82, 336–339. doi: <https://doi.org/10.1016/j.ijrmhm.2019.05.010>
4. Jung, C.-H., Lee, S.-J. (2005). Machining of hot pressed alumina–boron carbide composite cutting tool. *International Journal of Refractory Metals and Hard Materials*, 23 (3), 171–173. doi: <https://doi.org/10.1016/j.ijrmhm.2005.02.001>
5. Gevorkyan, E., Mamalis, A., Vovk, R., Semiatkowski, Z., Morozow, D., Nerubatskyi, V., Morozova, O. (2021). Special features of manufacturing cutting inserts from nanocomposite material Al₂O₃-SiC. *Journal of Instrumentation*, 16 (10), P10015. doi: <https://doi.org/10.1088/1748-0221/16/10/p10015>
6. Suzuki, K. (1984). The current state of ceramic tools and trends in its development in the future. *Seramikusu*, 19 (17), 542–556.
7. Raychenko, A. I. (1987). Vliyanie skorosti nagreva na poroobrazovanie v ul'tradisperstnyh poroshkah. *Metallurgiya*, 5, 14–18.
8. Peres, V., Favergeon, L., Andrieu, M., Palussière, J. C., Bolland, J., Delafay, C., Pijolat, M. (2012). High temperature chromium volatilization from Cr₂O₃ powder and Cr₂O₃-doped UO₂ pellets in reducing atmospheres. *Journal of Nuclear Materials*, 423 (1-3), 93–101. doi: <https://doi.org/10.1016/j.jnucmat.2012.01.001>
9. Hevorkian, E. S., Nerubatskyi, V. P. (2009). Do pytannia otrymannia tonkodispersnykh struktur z nanoporoshkiv oksydu aliuminiu. *Zbirnyk naukovykh prats Ukrainkoi derzhavnoi akademiyi zaliznychnoho transportu*, 111, 151–167. Available at: <http://lib.kart.edu.ua/handle/123456789/4418>
10. Zaloha, V. O., Honcharov, V. D., Zaloha, O. O. (2013). Suchasni instrumentalni materialy u mashynobuduvanni. Sumy: Sumskyi derzhavnyi universytet, 371. Available at: <http://library.ztu.edu.ua/e-copies/books/zaloga28.pdf>
11. Tkachenko, Y. G., Yurchenko, D. Z., Koval'chenko, M. S. (2008). High-temperature friction of refractory compounds. *Powder Metallurgy and Metal Ceramics*, 47 (1-2), 129–136. doi: <https://doi.org/10.1007/s11106-008-0018-z>
12. Gevorkyan, E., Nerubatskyi, V., Gutsalenko, Y., Melnik, O., Voloshyna, L. (2020). Examination of patterns in obtaining porous structures from submicron aluminum oxide powder and its mixtures. *Eastern-European Journal of Enterprise Technologies*, 6 (6 (108)), 41–49. doi: <https://doi.org/10.15587/1729-4061.2020.216733>
13. Grubiy, S. V. (2008). *Metody optimizacii rezhimnykh parametrov lezvynoy obrabotki*. Moscow: MGTU im. N. E. Baumana, 94.
14. Zhed', V. P., Borovskiy, G. V., Muzykant, Ya. A., Ippolitov, I. M. (1987). *Rezhushchie instrumenty, osnashchennye sverhtverdymi i keramicheskimi materialami i ih primenenie*. Moscow: Mashinostroenie, 320.
15. Gevorkyan, E., Rucki, M., Sałaciński, T., Siemiątkowski, Z., Nerubatskyi, V., Kucharczyk, W. et. al. (2021). Feasibility of Cobalt-Free Nanostructured WC Cutting Inserts for Machining of a TiC/Fe Composite. *Materials*, 14 (12), 3432. doi: <https://doi.org/10.3390/ma14123432>
16. Norfauzi, T., Hadzley, A., Azlan, U., Afuza, A., Faiz, M., Naim, M. (2019). Fabrication and machining performance of ceramic cutting tool based on the Al₂O₃-ZrO₂-Cr₂O₃ compositions. *Journal of Materials Research and Technology*, 8 (6), 5114–5123. doi: <https://doi.org/10.1016/j.jmrt.2019.08.034>
17. Azhar, A. Z. A., Hadzley, M., Tamin, N., Azlan, U. A. A., Hassan, M. H. (2020). Friction and wear analysis of ceramic cutting tool made from Alumina-Zirconia-Chromia. *Jurnal Tribologi*, 24, 27–38. Available at: https://www.researchgate.net/publication/344469179_Friction_and_wear_analysis_of_ceramic_cutting_tool_made_from_Alumina-Zirconia-Chromia
18. Mudzaffar, R. N., Bahauddin, M. F. I., Manshor, H., Azhar, A. Z. A., Rejab, N. A., Ali, A. M. (2021). Wear performance of the zirconia toughened alumina added with TiO₂ and Cr₂O₃ ceramic cutting tool. *Research Square*. doi: <https://doi.org/10.21203/rs.3.rs-956224/v1>
19. Gevorkyan, E., Nerubatskyi, V., Chyshkala, V., Morozova, O. (2021). Revealing specific features of structure formation in composites based on nanopowders of synthesized zirconium dioxide. *Eastern-European Journal of Enterprise Technologies*, 5 (12 (113)), 6–19. doi: <https://doi.org/10.15587/1729-4061.2021.242503>
20. Adel, S., Cherifa, B., Elhak, D. D., Mounira, B. (2018). Effect of Cr₂O₃ and Fe₂O₃ doping on the thermal activation of un-polarized PZT charge carriers. *Boletín de La Sociedad Española de Cerámica y Vidrio*, 57 (3), 124–131. doi: <https://doi.org/10.1016/j.bsecv.2017.11.001>
21. Gayo, G. X., Lavat, A. E. (2018). Green ceramic pigment based on chromium recovered from a plating waste. *Ceramics International*, 44 (18), 22181–22188. doi: <https://doi.org/10.1016/j.ceramint.2018.08.336>

22. Grigoriev, S. N., Fedorov, S. V., Hamdy, K. (2019). Materials, properties, manufacturing methods and cutting performance of innovative ceramic cutting tools – a review. *Manufacturing Review*, 6, 19. doi: <https://doi.org/10.1051/mfreview/2019016>
23. Cui, S., Liu, Y., Wang, T., Tieu, K., Wang, L., Zeng, D. et. al. (2021). Tribological behavior comparisons of high chromium stainless and mild steels against high-speed steel and ceramics at high temperatures. *Friction*. doi: <https://doi.org/10.1007/s40544-021-0509-1>
24. Gevorkyan, E. S., Nerubatskiy, V. P., Chyshkala, V. O., Morozova, O. M. (2020). Aluminum oxide nanopowders sintering at hot pressing using direct current. *Modern scientific researches*, 14 (1), 12–18. Available at: <http://repo.knmu.edu.ua/bitstream/123456789/28055/1/An%20article.pdf>
25. Chyshkala, V. O., Lytovchenko, S. V., Gevorkyan, E. S., Nerubatskiy, V. P., Morozova, O. M. (2021). Structural phase processes in multicomponent metal ceramic oxide materials based on the system Y–Ti–Zr–O (Y_2O_3 – TiO_2 – ZrO_2). *SWorldJournal*, 7 (1), 17–31. Available at: <http://repo.knmu.edu.ua/bitstream/123456789/29367/1/SworlJjournal03.21%20%281%29.pdf>
26. Higashino, Y., Yamauchi, M., Goto, T., Nagasawa, T. (2003). Evaluation of Brittleness of Porcelain Fused to Pure Titanium by Fracture Toughness, Hardness and Fracture Energy. *Dental Materials Journal*, 22 (4), 532–542. doi: <https://doi.org/10.4012/dmj.22.532>
27. Quinn, G. D. (2006). Fracture Toughness of Ceramics by the Vickers Indentation Crack Length Method: A Critical Review. *Ceramic Engineering and Science Proceedings*, 45–62. doi: <https://doi.org/10.1002/9780470291313.ch5>
28. Rudenko, V. M. (2012). *Matematychna statystyka*. Kyiv: Tsentr uchbovoi literatury, 304. Available at: https://shron1.chtyvo.org.ua/Rudenko_Volodymyr/Matematychna_statystyka.pdf
29. Ishchenko, O. V., Mykhalchuk, V. M., Bila, N. I., Haidai, S. V., Bilyi, O. V. (2012). *Statystychni metody u khimiyi*. Donetsk: Vydavnytstvo DonNU, 504. Available at: https://physchem.knu.ua/materials/GI_1-3.pdf
30. Storchak, M., Zakiev, I., Träris, L. (2018). Mechanical properties of subsurface layers in the machining of the titanium alloy $Ti_{10}V_2Fe_3Al$. *Journal of Mechanical Science and Technology*, 32 (1), 315–322. doi: <https://doi.org/10.1007/s12206-017-1231-9>
31. Vasylyev, M. A., Mordiyuk, B. N., Sidorenko, S. I., Voloshko, S. M., Burmak, A. P., Kruhlov, I. O., Zakiev, V. I. (2019). Characterization of ZrN coating low-temperature deposited on the preliminary Ar^+ ions treated 2024 Al-alloy. *Surface and Coatings Technology*, 361, 413–424. doi: <https://doi.org/10.1016/j.surfcoat.2018.12.010>
32. Mechnik, V. A., Bondarenko, N. A., Kolodnitskiy, V. M., Zakiev, V. I., Zakiev, I. M., Storchak, M. et. al. (2019). Physico-mechanical and Tribological Properties of Fe-Cu-Ni-Sn and Fe-Cu-Ni-Sn-VN Nanocomposites Obtained by Powder Metallurgy Methods. *Tribology in Industry*, 41 (2), 188–198. doi: <https://doi.org/10.24874/ti.2019.41.02.05>
33. Kirichek, T. Yu., Korotenko, Ye. V. (2016). Usage of contact and noncontact profilometrical methods for investigation of intaglio printing surfaces. *Trudy BGTU*, 9, 16–21. Available at: <https://elib.belstu.by/bitstream/123456789/20371/1/3Kirichek.pdf>
34. Leonenko, P. V., Zakiev, I. M., Gogotsi, G. A. (2013). Evaluation of surface quality of dental implants using non-contact 3D interferometric profilometer. *NMAPO imeni P. L. Shupyka*, 22 (4), 99–109. Available at: <http://ir.nmapo.edu.ua:8080/jspui/bitstream/lib/911/1/Evaluation%20of%20surface%20quality%20of%20dental%20implants.pdf>
35. Wu, C.-M., Cheng, Y.-C., Lai, W.-Y., Chen, P.-H., Way, T.-D. (2020). Friction and Wear Performance of Staple Carbon Fabric-Reinforced Composites: Effects of Surface Topography. *Polymers*, 12 (1), 141. doi: <https://doi.org/10.3390/polym12010141>
36. Chyshkala, V. O., Lytovchenko, S. V., Gevorkyan, E. S., Nerubatskiy, V. P., Morozova, O. M. (2021). Mastering the processes of synthesis of oxide compounds with the use of a powerful source of fast heating of the initial ingredients. *Collected Scientific Works of Ukrainian State University of Railway Transport*, 196, 118–128. doi: <https://doi.org/10.18664/1994-7852.196.2021.242226>
37. Yust, C. S., Leitnaker, J. M., Devore, C. E. (1988). Wear of an alumina-silicon carbide whisker composite. *Wear*, 122 (2), 151–164. doi: [https://doi.org/10.1016/0043-1648\(88\)90075-0](https://doi.org/10.1016/0043-1648(88)90075-0)
38. Gevorkyan, E., Rucki, M., Krzysiak, Z., Chishkala, V., Zurowski, W., Kucharczyk, W. et. al. (2021). Analysis of the Electroconsolidation Process of Fine-Dispersed Structures Out of Hot Pressed Al_2O_3 –WC Nanopowders. *Materials*, 14 (21), 6503. doi: <https://doi.org/10.3390/ma14216503>
39. Azhar, A. Z. A., Choong, L. C., Mohamed, H., Ratnam, M. M., Ahmad, Z. A. (2012). Effects of Cr_2O_3 addition on the mechanical properties, microstructure and wear performance of zirconia-toughened-alumina (ZTA) cutting inserts. *Journal of Alloys and Compounds*, 513, 91–96. doi: <https://doi.org/10.1016/j.jallcom.2011.09.092>
40. Hirata, T., Akiyama, K., Yamamoto, H. (2000). Sintering behavior of Cr_2O_3 – Al_2O_3 ceramics. *Journal of the European Ceramic Society*, 20 (2), 195–199. doi: [https://doi.org/10.1016/S0955-2219\(99\)00161-2](https://doi.org/10.1016/S0955-2219(99)00161-2)
41. Bugrov, A. N., Al'myasheva, O. V. (2011). Formirovanie nanochastich Cr_2O_3 v gidrotermal'nykh usloviyah. *Nanosistemy: fizika, himiya, matematika*, 2 (4), 126–132. Available at: https://www.researchgate.net/publication/286779209_Formirovanie_nanochastich_Cr2O3_v_gidrotermalnykh_usloviyah
42. Ryabchikov, I. V., Mizin, V. G., Yarovoi, K. I. (2013). Reduction of iron and chromium from oxides by carbon. *Steel in Translation*, 43 (6), 379–382. doi: <https://doi.org/10.3103/S096709121306017x>
43. Kamkina, L. V., Nadtochiy, A. A., Ankudinov, R. V., Hryshyn, A. M. (2015). *Osnovy dysotsiatsiyi ta horinnia spoluk*. Dnipropetrovsk: NMetAU, 70. Available at: https://nmetau.edu.ua/file/osnovi_dissots_i_gorinnya_spoluk.2015.pdf
44. Latu-Romain, L., Mathieu, S., Vilasi, M., Renou, G., Coindeau, S., Galerie, A., Wouters, Y. (2016). The Role of Oxygen Partial Pressure on the Nature of the Oxide Scale on a NiCr Model Alloy. *Oxidation of Metals*, 88 (3-4), 481–493. doi: <https://doi.org/10.1007/s11085-016-9670-8>

45. Gevorkyan, E. S., Nerubatskiy, V. P., Chyshkala, V. O., Morozova, O. M. (2021). Cutting composite material based on nanopowders of aluminum oxide and tungsten monocarbide. *Modern engineering and innovative technologies*, 15 (2), 6–14. Available at: <https://www.moderntechno.de/index.php/meit/issue/view/meit15-02/meit15-02>
46. Serbenyuk, T. B., Aleksandrova, L. I., Zaika, M. I., Ivzhenko, V. V., Kuz'menko, E. F., Loshak, M. G. et. al. (2008). Structure, mechanical and functional properties of aluminum nitride-silicon carbide ceramic material. *Journal of Superhard Materials*, 30 (6), 384–391. doi: <https://doi.org/10.3103/s106345760806004x>
47. Chasnyk, V., Chasnyk, D., Fesenko, I., Kaidash, O., Turkeych, V. (2021). Dielectric characteristics of pressureless sintered AlN-based composites in the 3–37 GHz frequency range. *Journal of Materials Science: Materials in Electronics*, 32 (2), 2524–2534. doi: <https://doi.org/10.1007/s10854-020-05019-6>
48. Strelou, K. K. (1985). *Teoreticheskie osnovy tehnologii ognepurnykh materialov*. Moscow: Metallurgiya, 480.
49. Ouensanga, A. (1987). High Temperature Thermodynamic Study of the Reduction of Cr₂O₃ by Graphite. *International Journal of Materials Research*, 78 (1), 70–72. doi: <https://doi.org/10.1515/ijmr-1987-780110>
50. Hevorkian, E. S., Nerubatskiy, V. P. (2009). Modeliuvannia protsesu hariachoho presuvannia Al₂O₃ pry priamomu propuskanni zminnoho elektrychnoho strumu z chastotoiu 50 Hts. *Zbirnyk naukovykh prats Ukrainskoi derzhavnoi akademiyi zaliznychnoho transportu*, 110, 45–52. Available at: <http://lib.kart.edu.ua/handle/123456789/4416>
51. Gevorkyan, E. S., Nerubatskiy, V. P., Mel'nik, O. M. (2010). Goryachee pressovanie nanoporoshkov sostava ZrO₂–5 %Y₂O₃. *Zbirnyk naukovykh prats Ukrainskoi derzhavnoi akademiyi zaliznychnoho transportu*, 119, 106–110.